論文 / 著書情報
Article / Book Information

Title	Long-Term Differential and Averaged Deformation of Box-Type Pre-stressed Concrete Exposed to Natural Environment
Authors	Nobuhiro Chijiwa, Shuntaro Hayasaka, Koichi Maekawa
Citation	Journal of Advanced Concrete Technology, Vol. 16, No. 1, pp. 1-17
Pub. date	2018, 1

Journal of Advanced Concrete Technology
Materials, Structures and Environment

Long-Term Differential and Averaged Deformation of Box-Type Pre-stressed Concrete Exposed to Natural Environment

Nobuhiro Chijiwa, Shuntaro Hayasaka, Koichi Maekawa
Journal of Advanced Concrete Technology, volume 16 (2018), pp. 1-17

Technical Report

Long-Term Differential and Averaged Deformation of Box-Type Pre-stressed Concrete Exposed to Natural Environment

Nobuhiro Chijiwa[1], Shuntaro Hayasaka[2] and Koichi Maekawa[3*]

Received 9 October 2017, accepted 4 January 2018 doi:10.3151/jact.16.1

Abstract

Middle-scale box-sectional hollow PC ducts, which consist of heterogeneous concrete with different mix proportions, were exposed to natural environments for about three years, and the long-term curvature and axial mean deformation, which have much to do with deflection of long span bridge viaducts, was gaged for verification of coupled thermo-hygral and multi-scale models. The associated internal moisture and the local climate inside micro-pores were measured and the effect of precipitation was quantified over yearly four seasons. The moisture migration linked with concrete multi-scale mechanics was analyzed and the simulation results are compared with the field exposure tests. The reliability of the thermo-hygral analysis, which has been used for estimating the long-term serviceability of bridges, was made firmer.

1. Introduction

Long-term excessive deflection of box-sectional hollow PC viaducts has been a key of structural serviceability design (Bazant *et al.* 2012, 2010; Watanabe *et al*. 2008; Hata *et al*. 1993; Kristek *et al.* 2006; Navrátil and Zich 2010) and its mechanism was investigated in view of coupled mechanics and thermodynamics of structural concrete (Ohno *et al.* 2012; Maekawa *et al.* 2012, 2011, 2008). The continued deflection for a long time is clarified mainly due to the differential shrinkage of viaduct's flanges of different dimensions (Maekawa *et al.* 2015). Currently, the long-term excessive deflection can be estimated by thermo-hygral analysis (Ishida *et al.* 2007; Maekawa *et al*. 2008; Yoneda *et al*. 2015, 2013) which simulates the moisture migration and equilibrium coupled with mechanical models as shown in **Fig. 1**.

The long-lasting deflection is predicted to finish almost 100 years after the construction, because the thermodynamic equilibrium of moisture between structural concrete and climate may be attained late in a while due to large sizes of flanges and webs of the bridge viaducts. But, it is hard to prove this prediction within the practical scale of time under ambient conditions. Furthermore, this simulation includes one assumption, that is to say, the top flange concrete is under the wetter condition by rain precipitation rather that the bottom flanges of the box viaducts. Although the multi-scale thermo-hygral modeling has been experimentally verified under stable conditions like in-door environments, its multi-scale overall verification for large-scale structures under natural out-door environments is further required for lifetime quality assurance over several decades (Rodrigues *et al.* 2010; Jauregui *et al*. 2003).

In this study, the authors investigate the applicability of the modeling to real climate conditions, and direct their attention to the middle scale mockup (approximately 1/4~1/5) of PC viaducts as shown in **Fig. 2**. The thermo-hygral events of moisture migration are thought to proceed higher by the square rate of the dimension (4×4=16, 5×5=25 times) than the one of real-scale infra-structures, because the moisture migration is not exactly but nearly governed by Poisson's type equation (Ishida *et al.* 2007). The shrinkage of concrete proceeds nonlinearly with moisture loss (Sakata 19893), and Kurihara *et al.* (2017) shows further magnified time-scale of drying shrinkage up to 100 times to attain the average shrinkage of concrete of 4~5 times dimensions. Thus, the moisture states and shrinkage which are attained about 100 years later will be realized about 3-5 years, as the size of the mockup is approximately 1/4~1/5 times different from the real long-span viaducts (See **Fig. 1**).

However, this rough estimate of time scale difference may not hold for lower water to cement ratio with autogenous shrinkage (Tazawa and Miyazawa 1995; Kim and Lee 1999; Lura *et al.* 2002), because moisture loss is comparatively less due to self-desiccation. Then, the authors also included the low water to cement ratio (W/C=28%) in experiments together with the chief target of normal concrete accompanying water loss by drying for a broad perspective of investigation.

2. Middle-scale mockup of PC viaduct

According to the practical time-scale and dimension of structural concrete (Weiss *et al.* 2000; Al-Saleh and Al-Zaidb 2006), segmental mockups of viaducts were designed. Five hollow box-sectional segments were serially assembled and axially pre-stressed as shown in **Fig. 3**. As the long-term deflection of real PC viaducts

[1]Associate Professor, Department of Civil Engineering, Tokyo Institute of Technology, Tokyo, Japan.
[2]Engineer, Kajima Corporation, Tokyo, Japan.
[3]Professor, Department of Civil Engineering, The University of Tokyo, Tokyo, Japan. *Corresponding author, *E-mail:* maekawa@concrete.t.u-tokyo.ac.jp

Table 1 Mix proportion of concrete used.

W/C (%)	s/a (%)	Air (%)	W (kg/m^3)	C (kg/m^3)	S (kg/m^3)	Lime stone powder(kg/m^3)	G (15-5mm) (kg/m^3)	G (20-15mm) (kg/m^3)	Admixture SP
28	40.1	4.5	168	600	642	0	437	533	5.7
40	45.3	4.5	168	420	794	0	437	533	3.57
50	49.2	4.5	168	336	899	0	422	515	2.18
60	51.7	4.5	168	288	809	120	407	497	2.45

may attribute to the differential shrinkage (Kim and Lee 1998) and creep over the sections (Ohno *et al.* 2012; Maekawa *et al.* 2015), the different thickness of upper and lower flanges was purposely made. Thus, the different shrinkage rate over flanges can be reproduced at site and is focused on in terms of transient curvature and the excessive deflection of box PC viaducts.

The authors installed another factor related to differential deformation, that is to say, the heterogeneous sections consisting of two kinds of concrete mixture with different water to cement ratios. Then, differential drying, autogenous shrinkage and creep lead to curvature which has much to do with the deflection of the ducts, and also the averaged axial deformation which is deeply related to loss of pre-stressing. For experimental verification, the sectional curvature as well as axial mean strain will be focused on.

The mix proportion of each concrete is lined up in **Table 1**. First, the bottom part of concrete was cast inside the formwork. Afterwards, the other mixture was monolithically cast on it. The segments were cured by lapping for a month and kept indoor until they were conveyed to

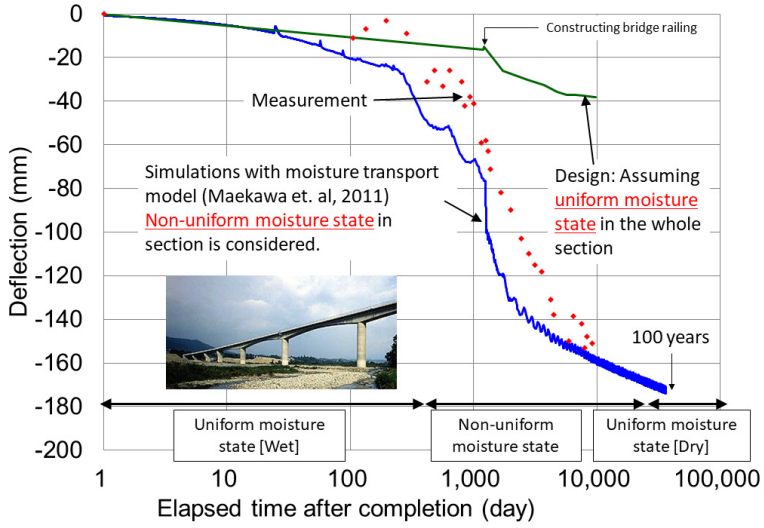

Fig. 1 Long-term deflection of box-type PC viaduct and simulation over several decades (Maekawa *et al.* 2015; Ohno *et al.* 2012; Watanabe *et al.* 2008).

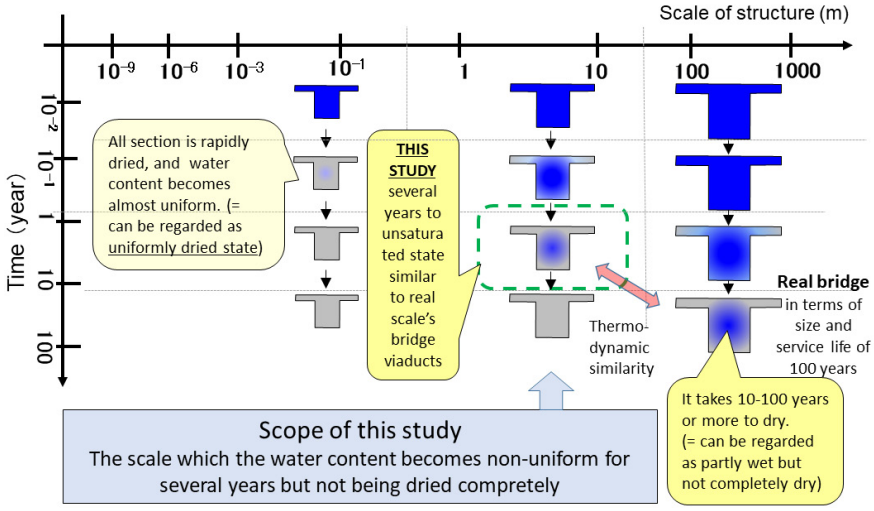

Fig. 2 Size of structural members and time-scale of thermodynamic process of drying.

the Kakioka testing site of The University of Tokyo as summarized in **Table 2**. Testing site is located about 100 km north from Tokyo Metropolis. **Figure 4** shows the site arrangement for the mockup specimens.

The strain transducers and strain gages were placed on reinforcing bars allocated at the center of each flange as shown in **Fig. 3**. The sensors to pick up temperature and relative humidity were embedded into the concrete of

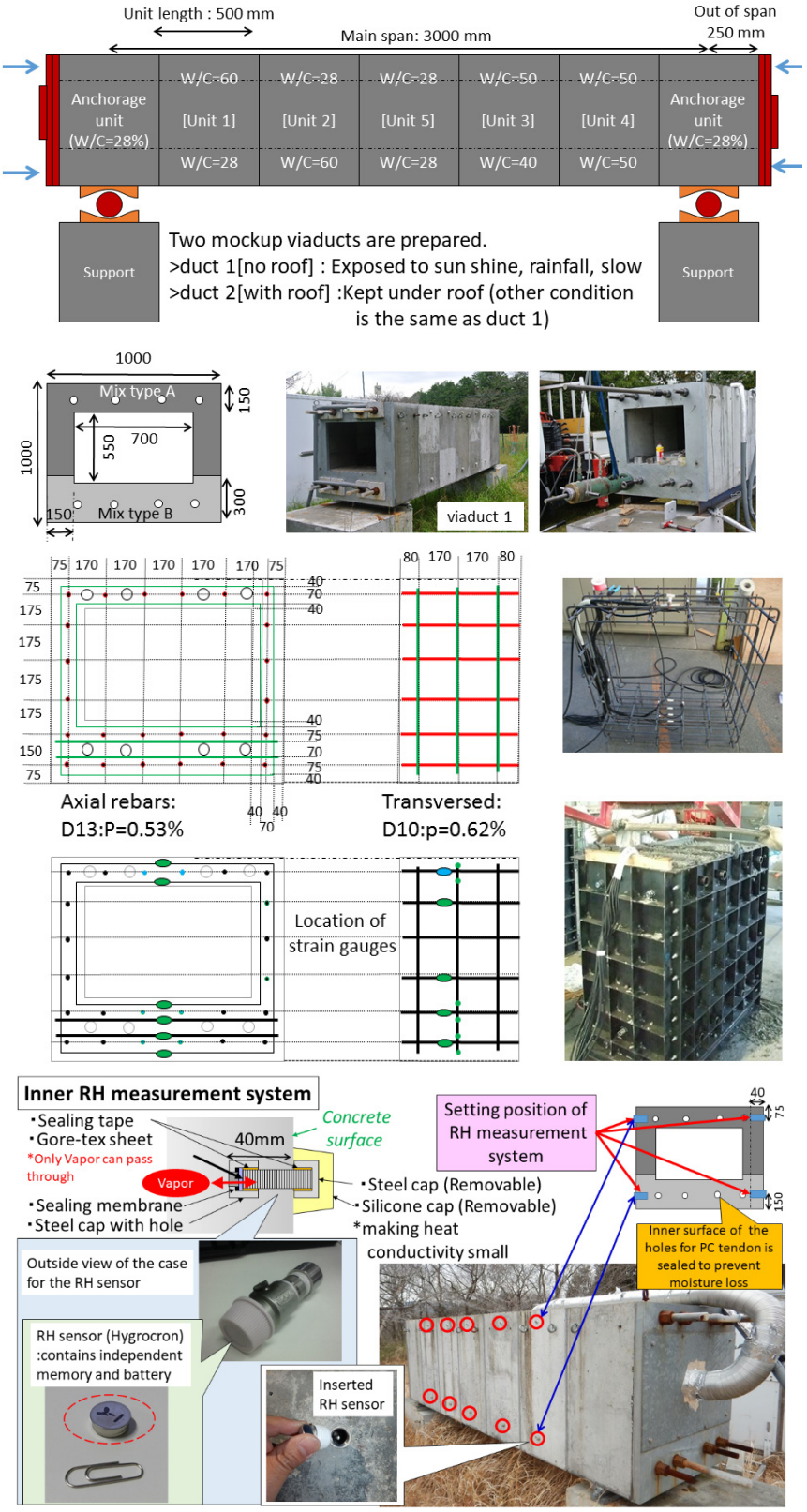

Fig. 3 PC mockup viaducts for multi-scale verification of thermo-hygral analysis.

Table 2 Periods of curing and pre-stressing.

		W/C (%)		Casting	End of curing	Pre-stressing	Loading level (Applied load (kN)) (Percentage to 28 day strength)	
		Upper flange	Bottom flange				Upper side	Bottom side
W / roof	Unit-1	60	28	2012/9/21	2012/10/24	2013/10/4	17 (1217)	6 (1948)
	Unit-2	28	60	2012/9/20	2012/10/24		5 (1217)	22 (1948)
	Unit-3	50	40	2012/8/24	2012/10/24		12 (1217)	11 (1948)
	Unit-4	50	50	2012/9/12	2012/10/24		12 (1217)	15 (1948)
	Unit-5	28	28	2012/9/16	2012/10/24		5 (1217)	6 (1948)
W / 0 roof	Unit-1	60	28	2013/2/28	2013/3/13		17 (1296)	6 (1988)
	Unit-2	28	60	2013/2/28	2013/3/13		5 (1296)	22 (1988)
	Unit-3	50	40	2012/8/24	2012/10/24		12 (1296)	11 (1988)
	Unit-4	50	50	2012/9/12	2012/10/24		12 (1296)	15 (1988)
	Unit-5	28	28	2012/9/16	2012/10/24		5 (1296)	6 (1988)

Note) Pre-stress temporally released on Nov. 24th 2014, and fully recovered on Dec. 12, 2014.
Note) A fire accident at the test site happened on March 17, 2014 and followed by electricity blackout.

both upper and lower flanges. The sensor head is protected by goa-text sheets through which the vapor can pass. For periodical replacement of batteries, no sealing with adhesive agent was made but a thin gap between concrete and the steel casing to support the sensor was allowed. The continuous measurement begun just before the casting of each segment.

All joint planes were sealed with water-proof agents and fresh paste was inserted in between segments for smooth and uniform touching of axial stresses. Afterwards, the pre-stressing was introduced, i.e., 1,200kN for the upper flange and 2,000kN for the lower one. Although the ambient conditions inside the box segments can be artificially controlled, this paper reports the cases where the inside of the box mockups was kept the same as the outside without any separation panel. The coupling of ambient conditions of inside and outside will be further discussed in another paper in future.

Figure 5 shows the climate states at the site and precipitation, which are used for the following analyses. This period was initially estimated to be necessary and sufficient to have quasi thermo-equilibrium equivalent to about 75 years of large-scale PC viaducts of 100m span-length (**Fig. 2**).

In order to examine the long-term moisture states in micro pores, roofs were placed above the mockup ducts so that they were not directly exposed to sunshine, rain fall nor snowing. Wind protection was not considered. According to the reports from the local metrological station, the annual wind speed was about 2m/sec during the site measurement.

3. Transient differential and mean strains of PC segments

The authors pay their attention to the differential deformation of both flanges over the section and the average axial strain of each segment for model verification. The former deformation is linear-proportional to the curvature related to long-term deflection of PC viaducts. The

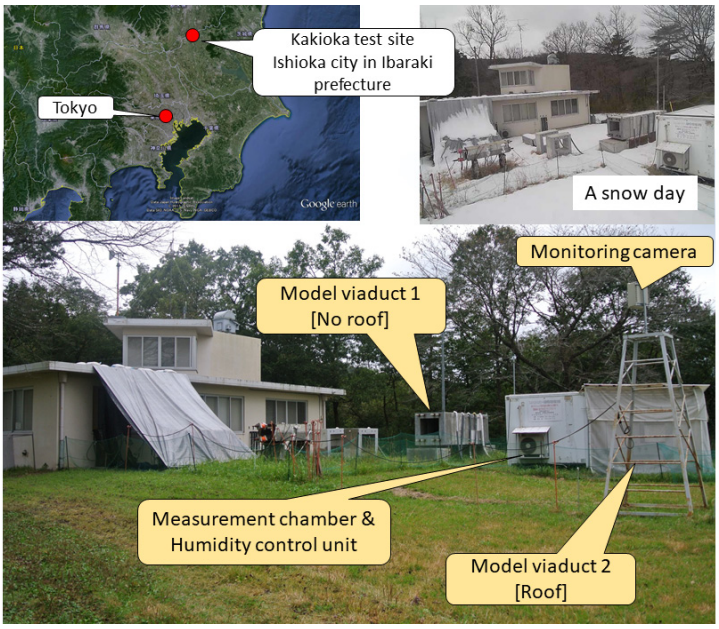

Fig. 4 Site for exposure experiments.

internal relative humidity inside the micro-pores of concrete was monitored as a parameter related to creep and shrinkage of concrete as well. We divide the differential strain of the upper and lower flanges by those distance to obtain the curvature according to in-plane hypothesis. The average strain is the mean value of the both flanges' strains.

For experimental verification of the thermo-hygral analysis associated with creep and shrinkage (Maekawa *et al*. 2015; Yoneda *et al.* 2015), absolute strains are reported in this study without any compensation of the thermal volumetric expansion and contraction. As the temperature of all specimens developed over the seasons almost uniformly, the measured differential strain is not influenced practically by the temperature changes, but it reflects the different evolution of creep and shrinkage of concrete.

The multi-scale hygral analysis (**Fig. 6**: Maekawa *et al.* 2008), which has been used for long-term serviceability simulation of real infrastructures (Ohno *et al.* 2012; Chijiwa *et al.* 2015; Chijiwa and Maekawa 2015), is also applied to the lifetime prediction of each segment (**Fig. 3**). Analysis begins just after mixing of fresh concrete and the hydration and micro-pore structure formation are traced step by step. Under the lapped curing, moisture loss through the surfaces is not computationally allowed. At the onset of exposure to out-door climate, the moisture transfer elements are placed on the surface and the moisture exchange between concrete and environments is made possible (Yoneda *et al.* 2015, 2013).

The loss of moisture stored in micro-pores creates capillary tension forces and the disjoining pressure. These micro-forces cause shrinkage of cement hydrated solids (Asamoto *et al*. 2008, 2006). Time dependent deformation of solid skeleton is also driven by these micro forces as well as the external mechanistic actions. Then, the thermo-hygral analysis does not need to define any creep and shrinkage separately as discussed by Pickett (1942) and Nagataki and Yonekura (1984). For the mockup of the PC duct, moisture states and micro-forces vary together with the sustained external forces by pre-stressing. Furthermore, the micro-pore structures were forced to be largely changed due to hydration reaction of cement. Thus, this differential deformation associated with the long-term deflection of bridges is of complexity to some extent and suitable for numerical model verification.

3.1 Preliminary experiment for precipitation boundary

The analytical point of this study is how to treat the precipitation including snow cover (Asamoto *et al.* 2011; Shimomura 2015). The upper surface of each segment was assumed to be exposed to the stagnant condensed water for every hour when it rains. For lifetime simulation, the authors use the precipitation data reported from

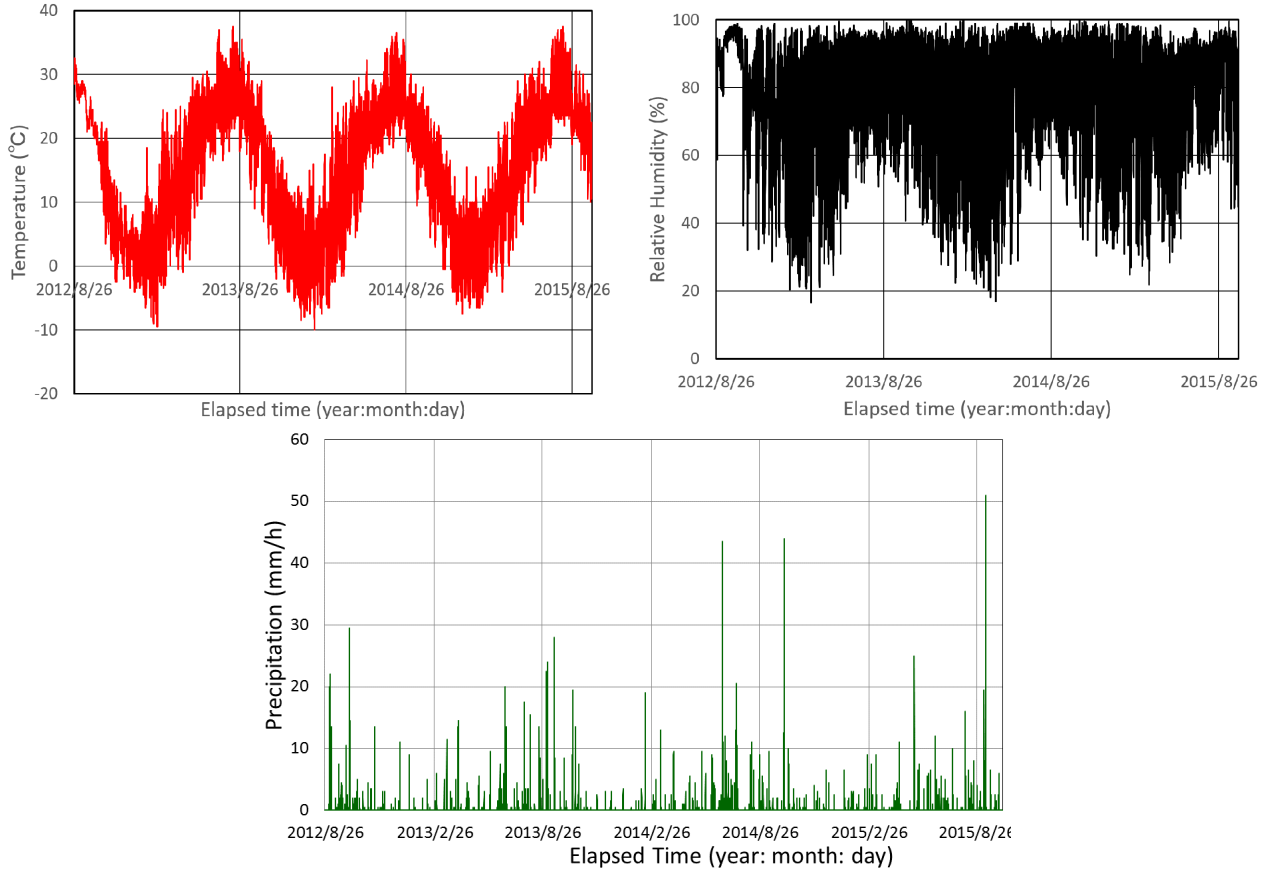

Fig. 5 Ambient conditions and precipitation.

Table 3 Mix proportion of mortar used.

W/C (%)	Air (%)	W (kg/m^3)	C (kg/m^3)	S (kg/m^3)
25	3	240	906	1152
50	3	319	638	1166

Kakioka Magnetic Observatory next to the test site. As for the snow cover, the report from Tsukuba Meteorological Observatory was used. During that time of precipitation and snow cover, 500 times of the vapor transfer coefficient for RH=99.9% is tentatively assumed to simply take into account the rapid convection of condensed water.

Here, the thermo-hygral model used in this study is built based upon the quasi-equilibrium states even for dynamic events as well as statics. In fact, the vapor transfer dynamics is slow and satisfies the quasi-equilibrated states for a while. The authors understand that rapid suction of condensed water at the rainfall and snow cover is being investigated at this moment in view of the nano-channel hydraulics (Han *et al.* 2017). Hereafter, we may tentatively apply magnified moisture transmission coefficient at the precipitation in order to simply consider the rapid suction as mentioned above.

For validating this practical method before the full-lifetime simulation, the authors carried out the quick absorption tests of cylinder specimens (see **Fig. 7**) and the exposure tests in using standard specimens (10x10x40cm) of the mortar as listed in **Table 3**. The weight gain of oven dried cylinders was measured under water so as to roughly obtain the magnification factor as stated above. Furthermore, specimens of standard prism were exposed to out-door environments in Tokyo for half a year, and the pore humidity of concrete just close to the surface as well as the gravity center was computed as shown in **Fig. 7**. As the specimen was placed just on the ground, the wind speed around the specimen was not computationally considered.

In the case of W/C=50%, the computed averaged relative humidity inside concrete gradually decreases due to drying up to 140 days after exposure (Andrade *et al.* 1999; Grasley *et al.* 2006). The gravity center of the specimen is almost wet at the beginning of exposure, but the effect of drying reaches at about 90 days and after 140 days, the relative humidity at the surface and the average becomes closer. It means that the moisture state comes up to the quasi-equilibrium of thermodynamics with the varying ambient conditions over the seasons. Concerning W/C=25%, however, the averaged relative humidity and that at the gravity center are similar owing to strong self-desiccation.

The computed transient shrinkage strain reasonably

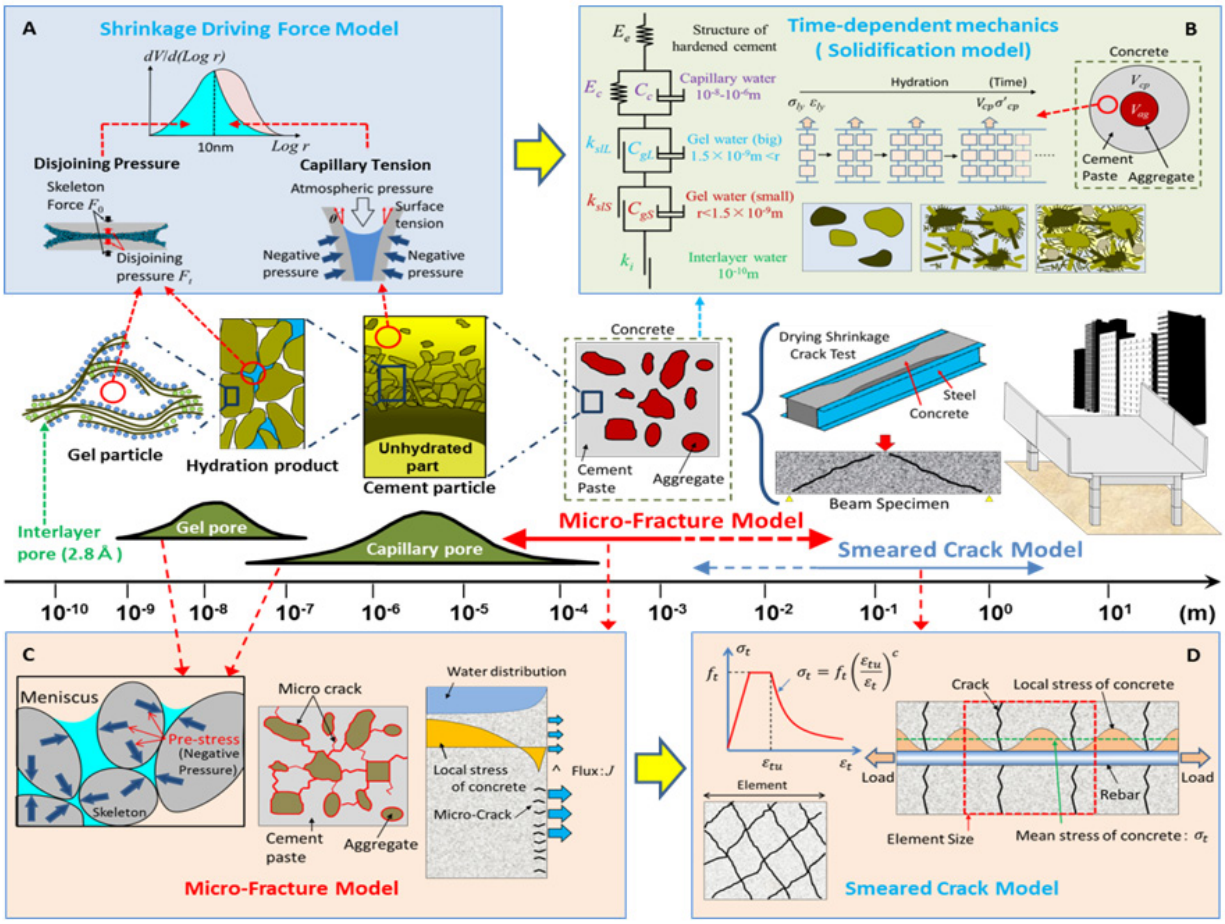

Fig. 6 Multi-scale framework for thermo-hygral analysis (Maekawa *et al.* 2015; Yoneda *et al.* 2015).

matches the experiments as shown in **Fig. 8**. It seems that the shrinkage would almost converge to the capacity around 140 days, and some volume recovery can be seen afterwards. This attributes to the moisture supply by the precipitation. In the case of W/C=50%, as unusual cracking of concrete occurred just close to the embedded strain gauge at 90 days, the shrinkage is relaxed due to self-equilibrated tension. It is thought that the local cracking would be introduced due to the presence of embedded gauge. As the un-cracked behaviors were well captured anyhow, the authors used the boundary condition as above for the long-term simulation of the box sectional segment.

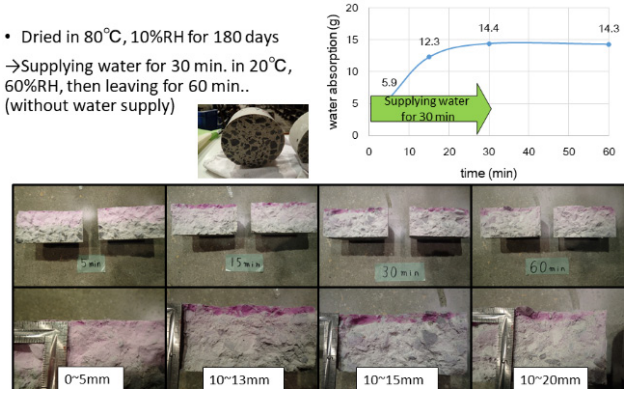

Preliminary cylinder test for rapid absorption

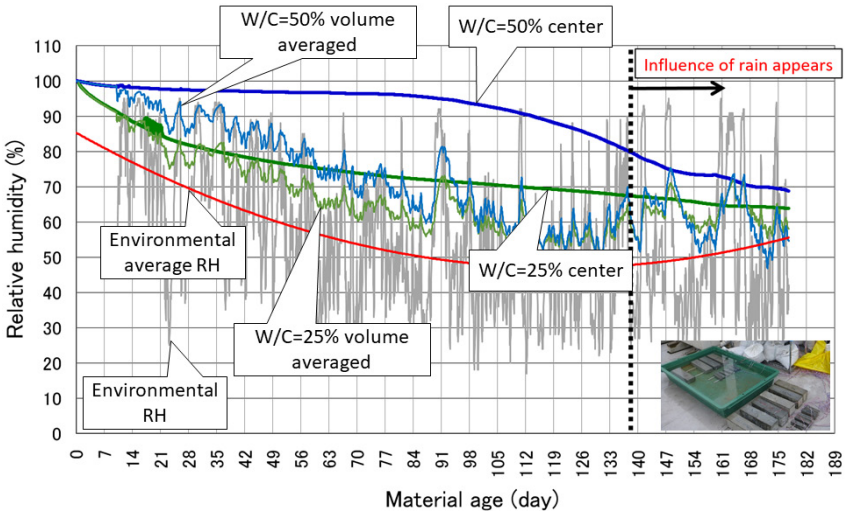

Preliminary test of standard prism for relative humidity

Fig. 7 Computed moisture humidity of referential specimens with precipitation.

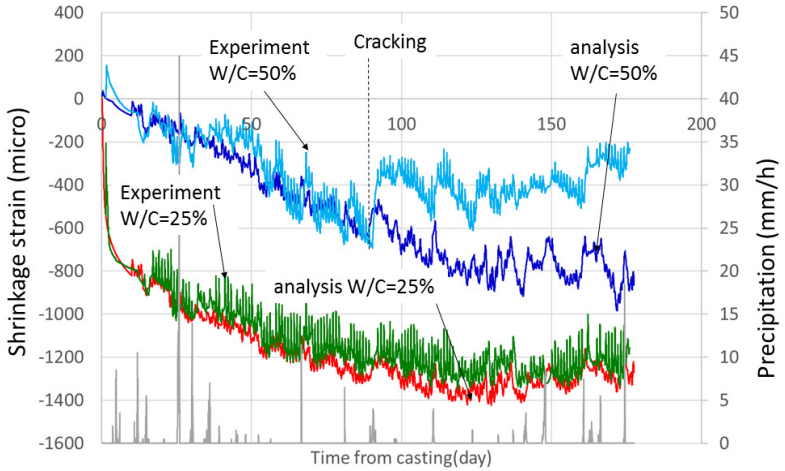

Fig. 8 Computed and measured shrinkage strains of reference specimens with precipitation.

3.2 Transient differential and averaged strains for monolithic segments

Figure 9 shows the transient relative humidity inside the upper and lower flanges (see **Fig. 3**) of the segment Uuit-4 and Unit-5 with roof (see **Table 2**). The whole section was monolithically made by the single mixture of concrete with W/C=28% and 50%, respectively. The embedded sensors needed to be replaced partway for periodical battery charge. At this time, entire sensor casings were exposed to ambient air and the measured relative humidity was quickly reduced. After the re-installation of the sensors, the gradual recovery of RH to the thermo-dynamic equilibrium was made and came up to the convergence inside the casing which contains the sensor. As the sensors directly exposed to rainfall stopped function regrettably for about half a year due to seepage of condensed water, this paper reports the reading by the sensors which were protected by the roof.

For the case of W/C=50%, the relative humidity of both flanges was gradually converging to about 85-90% RH. It must be noted that the annually averaged ambient relative humidity (about 65%) and that of micro-pores inside concrete differs from each other over three years. During the whole range of measurement, concrete of the lower flange was found to be a bit wetter than the one of the top flange even though the roof cover was facilitated. It is most probably due to the condensation on the bottom surface of the lower flange in the early morning of winter season, because the mockup was placed above the natural soil, which is a source of rising vapor mainly in winter.

For the case of W/C=28%, variation of moisture is generally similar to the case of W/C=50%, but its magnitude is a little smaller because of the self-desiccation, especially at the beginning of exposure at site. For all cases, it can be concluded that the relative humidity in micro-pores is greater than the annual average of atmosphere. If concrete would be kept indoor under constant ambient states, the humidity in micro-pores would be converged to them according to the second theorem of thermodynamics. Here, it must be noted that the measured relative humidity is thought not to be far from the local one at the sensor head, but it may not be the exact one because no perfect sealing against vapor transmission is possible to meet the periodical replacement of battery. This point shall be considered on discussing the model verification as follows.

Figure 10 shows the finite element discretization of each segment and their ambient boundary conditions. The upper flange's surface is assumed to be exposed to humid air as well as condensed water when rain fell according to the recorded climates as shown in **Fig. 5**. In accordance with the annual averaged wind speed (2.3m/sec) at site, the moisture emissivity coefficient with respect to the relative humidity (non-dimension) was assumed 5.0×10^{-5} [kg/m^2/sec] at the surfaces of flanges and side faces of the segment. The effect of precipitation was considered with the same manner as discussed in **Section 3.1**.

The side face of the segments was also attached to the condensed water when rail fell, but their surface was not exposed to stagnant water during the precipitation and rapid flow down of water was realized unlike the surface of the top flanges. After the rainfall, the side faces were

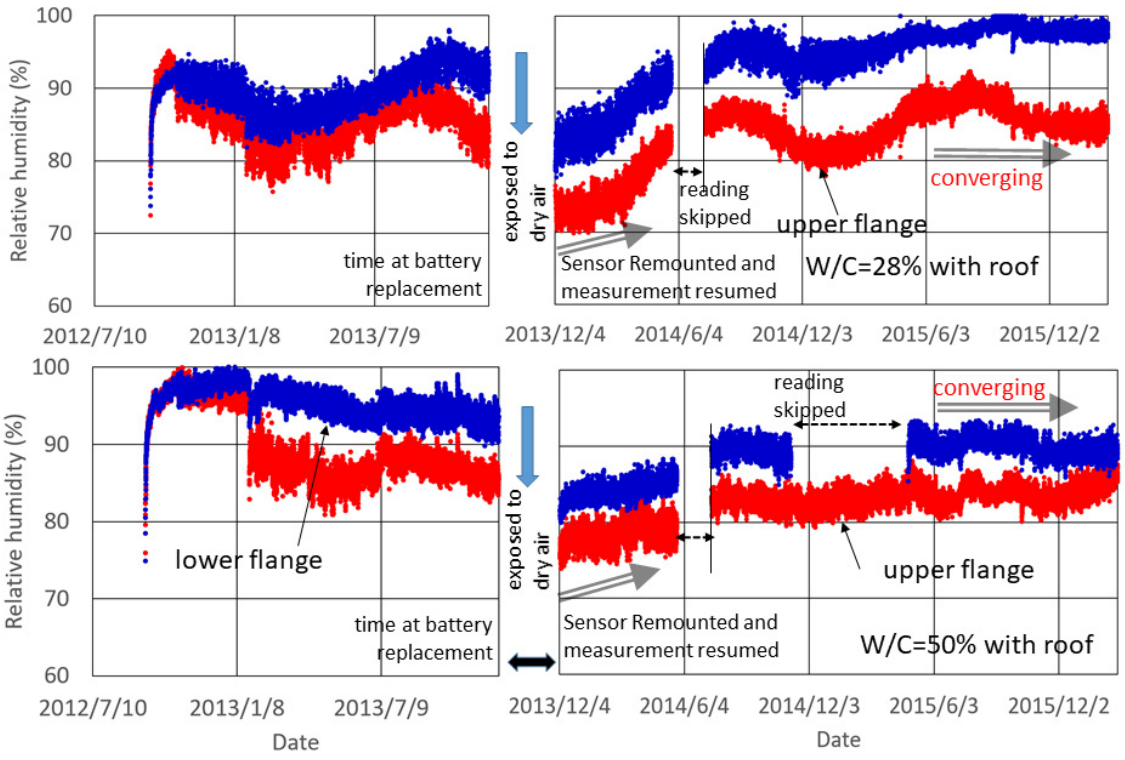

Fig. 9 Transient relative humidity inside the flanges.

quickly dried. Then, the authors set up the simple dry boundary conditions as the same as the surface of the bottom flange. In fact, the boundary condition of the side face has a little impact to the computed curvature of the segment of this paper's point.

Figure 11a shows the computed relative humidity inside the micro-pores, which is the primary factor of shrinkage and creep of concrete. The relative humidity just close to the surface of concrete (at 2.1mm) is almost the same as the ambient one. According to the depth from the surface, the daily fluctuation of the relative humidity reduces rapidly, and it varies smoothly as micro-climate of inside pores.

In comparison with the measurement as shown in **Fig. 9**, fluctuation of the sensed RH is more or less greater. It is thought that the extreme head of the sensor may capture some averaged relative humidity of the finite volume of sensor casing (**Fig. 11a**), because of the small gaps

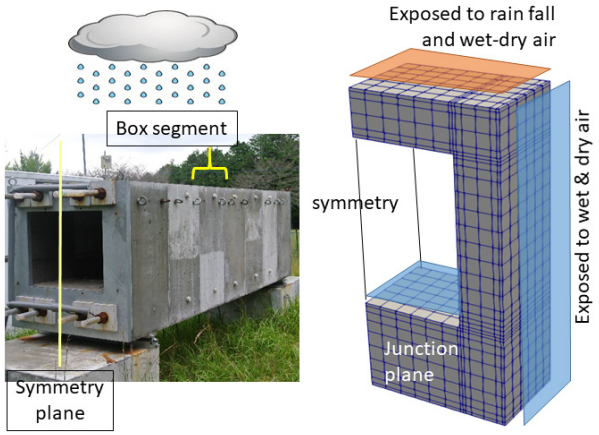

Fig. 10 Finite element discretization and ambient boundary conditions.

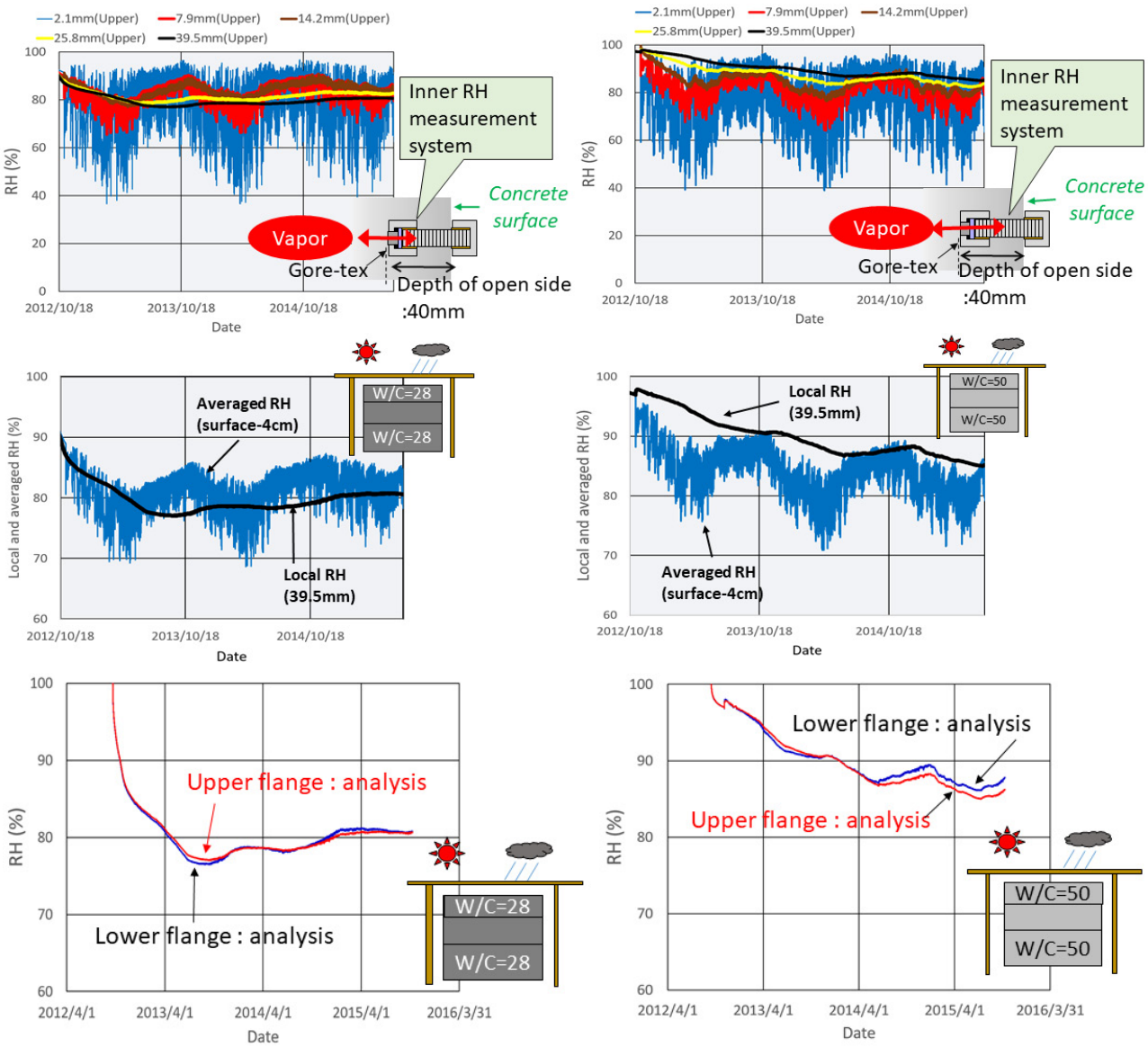

(a) Simulation on local and averaged RH simulation: covered by roof.

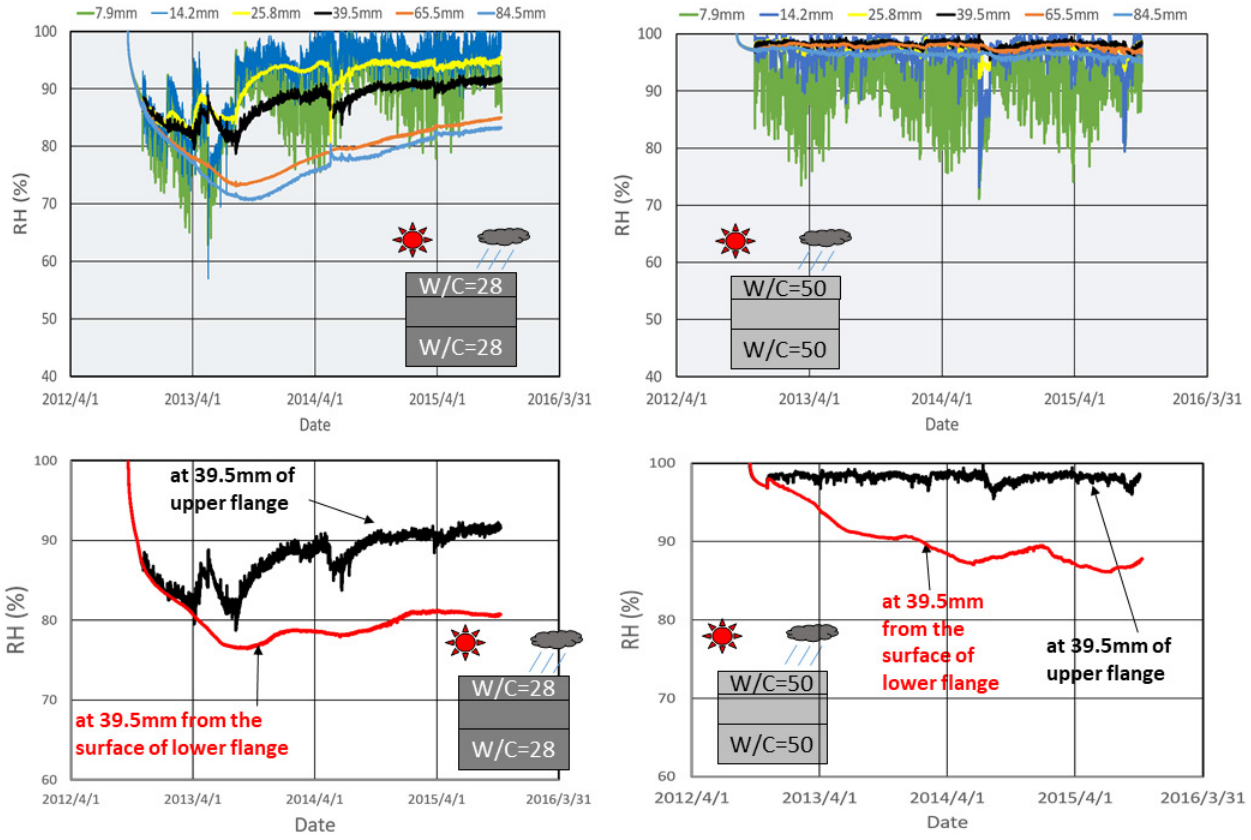

(b) Simulation on local and averaged RH simulation: covered by no roof.

Fig. 11 Computed relative humidity inside flanges.

remaining between concrete and the sensor casing for the sake of battery's replacement as mentioned previously. If the measured RH is in between the computed averaged relative humidity inside the sensor pipe (**Fig. 11a**) and the simulated local RH at the tip of the sensor, it seems that computed varying micro-climate inside concrete gets consistent with the reality.

Even though the rain does not reach the mockup, the relative humidity inside the flanges does not converge to the ambient average humidity and temperature (72.6% & 14.2℃) within the period of three years' exposure, but roughly speaking, it seems to come close to 90% for the case of W/C=50%. This simulation roughly matches the observation, and can predict that for the case of W/C=28%, the converged relative humidity is a little bit less than the one of W/C=50% owing to the self-desiccation. Since the section is monolithic and apart from precipitation, the computed relative humidity of inside concrete for upper and lower flanges is equal.

Figure 11b shows the computed averaged and local relative humidity at the center of the upper flange without roof (direct rainfall). In the case of W/C=28%, the rapid drop of the relative humidity inside the flanges is reproduced owing to the self-desiccation followed by the gradual recovery. When the mockup is exposed to the rainfall, the relative humidity of the upper flange computationally rises gradually owing to the intake of the condensed water. As a result, the drying shrinkage impact will be relaxed in terms of the curvature. In the case of W/C=50%, the gradual reduction of the relative humidity is seen because of less self-desiccation. The drying effect does not deeply penetrates but concrete is kept rather wet because of coarser micro-structures of hardened concrete.

Figure 12 shows the results of Unit-4 and Unit-5. As both upper and lower flanges of these cases consist of the same concrete mixture, the effect of autogenous shrinkage on the warping at early ages is negligible but pure axial contraction takes place. In analysis, the origin of differential strain was defined at the time when the site measurement started, and the one of experiment was at the time of fresh concrete casting. Then, the analytical and experimental warping just at the start of site measurement has some differences, inevitably.

The warping of the case of W/C=50% with roof (**Fig. 12a**), which has less self-desiccation and autogenous shrinkage, is solely caused by the flanges' thickness as the same mechanical properties of concrete can be assumed. In fact, the downward warping (negative differential strain) was created owing to the different rate of moisture loss and associated shrinkages of flanges. Furthermore, it is clarified that the effect of rain fall is not negligible as the case of no roof indicates. These facts of Unit-4 are associated with the long-term excessive deflection of real-scale box sectional PC viaducts (Maekawa *et al.* 2015; Ohno *et al.* 2012; Watanabe *et al.*

2008) as stated in Chapter 1 and Chapter 2. It is experimentally confirmed that the different shrinkage of top and bottom flanges rooted in the thickness as well as the ambient states has to be considered for the long-term prediction of deflection.

The mechanistic behaviors of Unit-5 with W/C=28% (**Fig. 12b**) are qualitatively similar to the case of Unit-4, but the magnitude of impact of flange thickness and the precipitation is much less and stable. Owing to the self-desiccation and autogenous shrinkage, moisture loss is quite less and the averaged shrinkage of flanges is hardly affected by their sizes, and dense pore structure does not allow quick seepage of condensed water as well. Then, it is thought that the long-term deflection of PC viaduct would be suppressed provided that very low W/C concrete would be applied. This view will be a future discussion. Unit-4 and Unit-5 are appropriate to mainly verify the concrete creep because of the uniform material properties over the section, and the thermo-hyrax modeling may capture the overall transition of average axial strain.

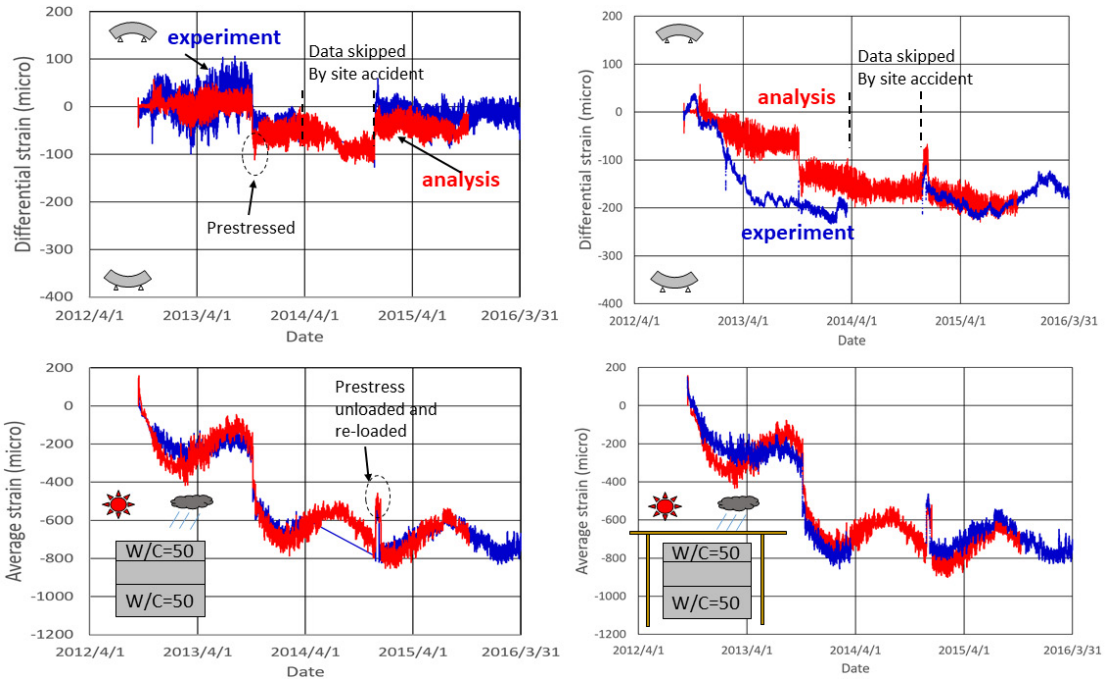

(a) Averaged and differential strains for W/C=50%

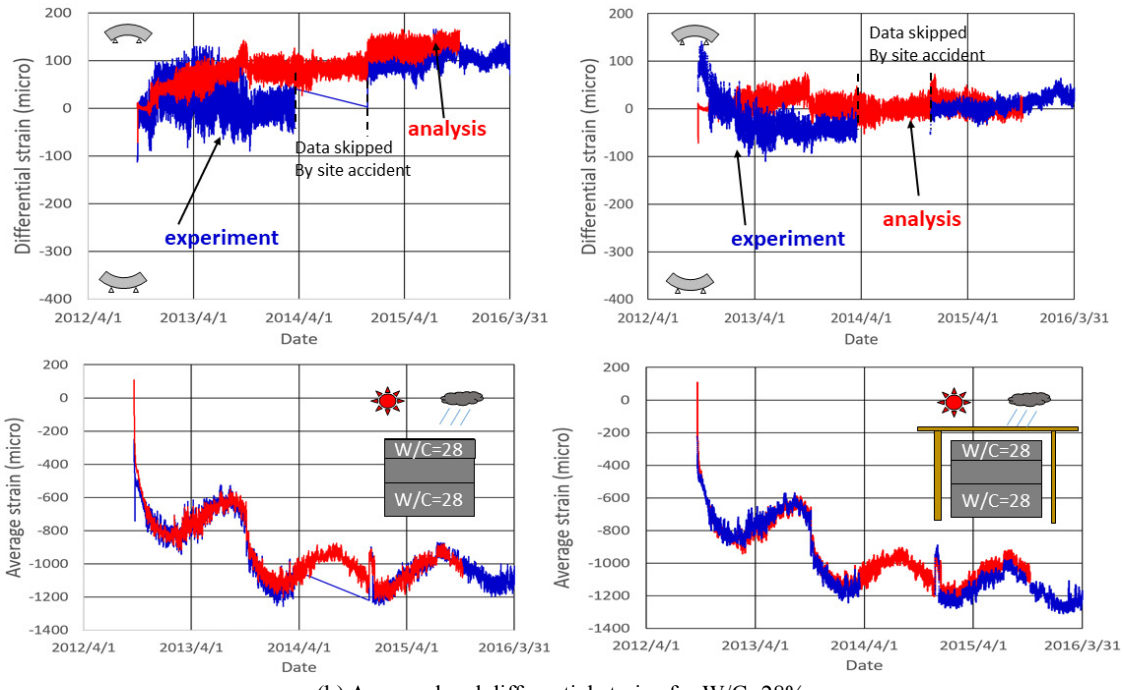

(b) Averaged and differential strains for W/C=28%

Fig. 12 Transient sectional curvature and the average axial strain caused by dimensioning of box sections.

3.3 Varying averaged and differential strains for heterogeneous segment

Figure 13 shows the transition of the curvature and the average axial strains with and without roof cover. The internal humidity profile of the box viaduct's mockup is illustrated as well. The differential strain (proportional to section-curvature) increased at once due to pre-stressing on October 4, 2013. This is the elastic deformation. After the anchorage of PC bars, the differential and the average strains gradually varied as time passed. Due to the roof coverage, no rain nor snow fell on the mockup. Then, the moisture of the upper flange is not fully saturated, but closer to 90% as shown in **Fig. 9**. Since the self-desiccation proceeds for the case of W/C=28%, the relative humidity of inside concrete is smaller compared to other places.

As shown in **Fig. 13a**, the upward warping of Unit-1 with roof is highly governed by the shrinkage of the bottom flange with larger sectional area. Especially, the greater upward warping was made by the early aged autogenous shrinkage. Afterwards, rapidly induced warping, as indicated by differential strains of the upper and lower flanges, was being recovered gradually due to the delayed drying shrinkage of the upper flange. After about three years, the curvature and the average axial strains of the segment Unit-1 seems to be stable. At this stage, the moisture condition is thought to reach the stability as well. The lower flange has a little bit drier than the upper one. To some extent, the behavioral simulation by the thermo-hygral analysis may capture the reality.

Compared to the transient average strains, the differential strain which creates sectional curvature looks a little far off the observation, especially when the prestress was introduced as indicated in **Fig. 13a**. Then, a further close-up view of the authors is directed to the absolute strains of both flanges as shown in **Fig. 13b**. Although the instantaneous differential strain comparatively differs from the experimental fact, the instantaneous elastic responses of the upper and bottom flanges match the reality. Then, the instantaneous stiffness is well simulated. It is understood as the statistics tells us that smaller deviation of local strains is somewhat magnified in the process of differentiation.

The effect of precipitation can be seen in **Fig. 13c** for the case of no roof for Unit-1. This material age of this specimen at pre-stressed was 5 month younger than the one of the Unit-1 with roof. The initially induced upward warping was almost the same as the case of **Fig. 13a**, because the driving force comes from the early aged autogenous shrinkage. However, the recovery of warping was suppressed substantially. It is thought that the rain-induced rapid water suction inhibits shrinkage of the top flange concrete. In fact, the moisture content of the top flange concrete was greater than that of the roof condition. We have the same story for the transition of the average axial strain as well.

Figure 14a shows the case of Unit-2 whose sectional composition is opposite to the case of Unit-1. Then, the direction of warping of the segment is opposite in nature. At the very beginning of observation, the downward warping was introduced mainly by the autogenous shrinkage similarly to the case of Unit-1, but the rate of recovery of warping was found slower as shown in **Fig. 14b**. The recovery of warping is mainly driven by the shrinkage of the flange with W/C=60%, because another flange of W/C=28% develops much stable volumetric shrinkage over the whole life of experiment as shown in **Fig. 12b**. Then, the difference from Unit-1 is associated with the thickness of the flange which drives the recovery of downward warping. Since the thickness of the flange of W/C=60% is large with slower water loss, the rate of shrinkage and corresponding warp recovery gets slow as presented by both experiment and analysis.

The magnitude of analytical warping recovery for the case of roof coverage is smaller than the reality. The tendency compared to the case of Unit-1 is well simulated but the curvature discrepancy of the roof case is not well understood. **Figure 14c** shows the computed and measured internal relative humidity of the bottom flange (W/C=60%) of Unit-2. Although the computed moisture state does not differ from the reality so much and this discrepancy is minor impact to the mechanistic responses as shown in **Fig. 14a**, some difference still remains. The authors think at this moment that the moisture emission coefficient concerning the local wind and the condensation will be one of possible factors of future improvement.

3.4 Proposal

Since rain falls on the upper flange, the internal relative humidity of concrete is close to 90-100% as almost saturated even in the case of W/C=28% and 60% for a long time. It means that three years climate action at the site in Japan may bring about quasi-saturation to concrete fully exposed to yearly precipitation regardless of micro-pore dimensions. This is the same boundary used in simulating the excessive deflection of the real PC bridge viaduct for more than 30 years (Maekawa *et al.* 2015; Ohno *et al.* 2012). Here, the authors want to raise a point that rainfall and snow cover shall be considered for structural maintenance & control (Chiu *et al*. 1996; Barr *et al.* 2005; Maaddawy *et al.* 2005) and the thermo-hygral analysis, which has been applied to the lifetime simulation of long-span bridges (Ohno *et al.* 2012; Maekawa *et al*. 2015), can be a new framework.

4. Conclusions

A series of exposure experiments to natural environments for the mockup of PC viaducts was performed for about four years including the preparation period at the test site, and the thermo-hygral and multi-scale modeling of mechanics are applied. Then, the following conclusions are earned as,

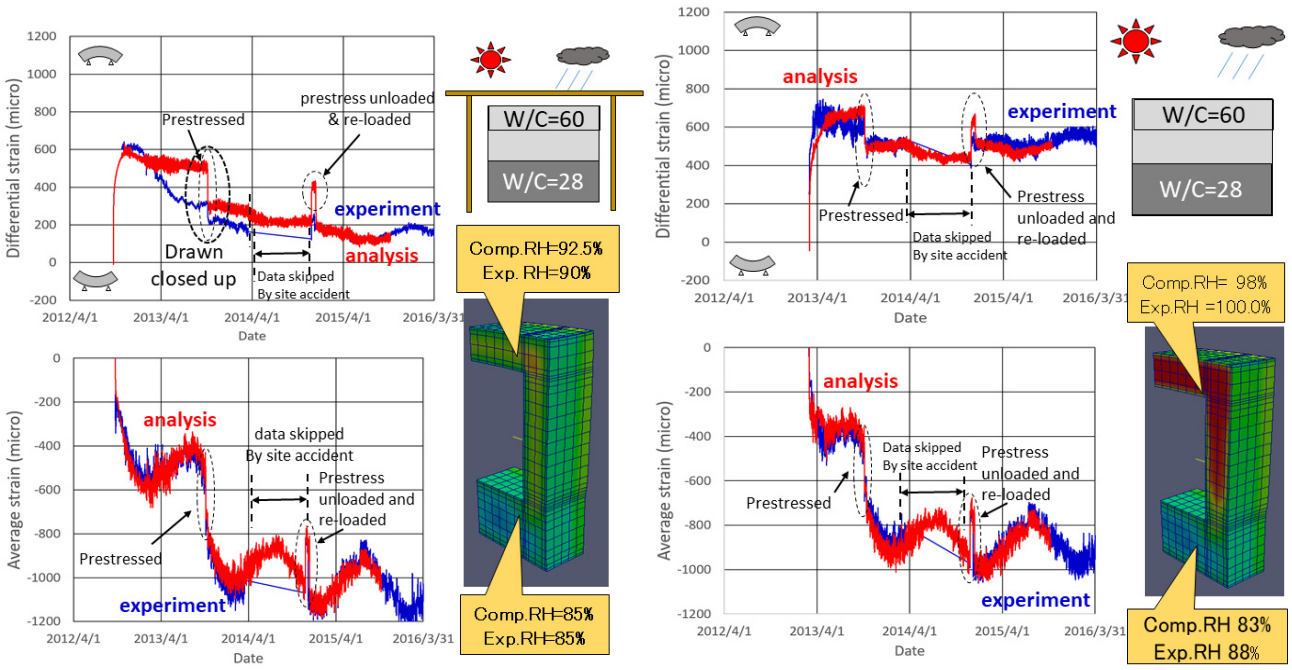

(a) Sectional deformation of Unit-1 with and without roof cover and the internal pore relative humidity at 39.5mm deep from the surface of flanges.

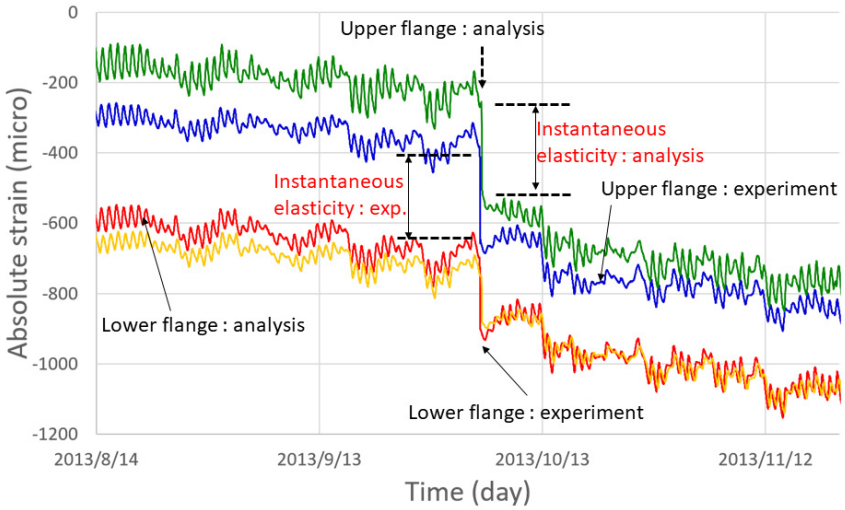

(b) Closed up of local strains for Unit-1 with roof.

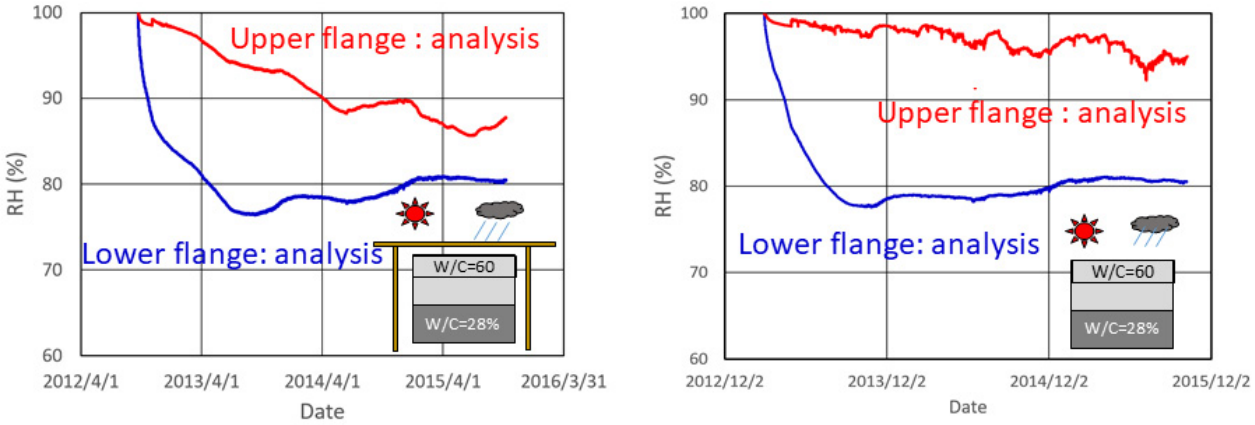

(c) Computes moisture state of micro-pores inside concrete of flanges.

Fig. 13 Transient differential and the average axial strains with the internal humidity inside mockup Unit-1.

(1) The curvature of box sectional PC hollow ducts was continuously measured and this differential deformation highly associated with the long-term deflection of bridges was quantitatively clarified to be influenced by the yearly precipitation. It implies that the ambient temperature and relative humidity alone are not enough to precisely estimate the serviceability of infrastructures in future, but the effect of stagnant water and snow cover shall be considered.

(2) The thermodynamic hygro-equilibrium inside concrete and associated convergence of differential deformation are attained about 3 years for the 1/5 scale-down mockup of PC viaducts as the multi-scale hygral analysis predicts. Accordingly, real-scale long-span PC bridge viaducts are estimated to reach the stability for 50~75 years under the

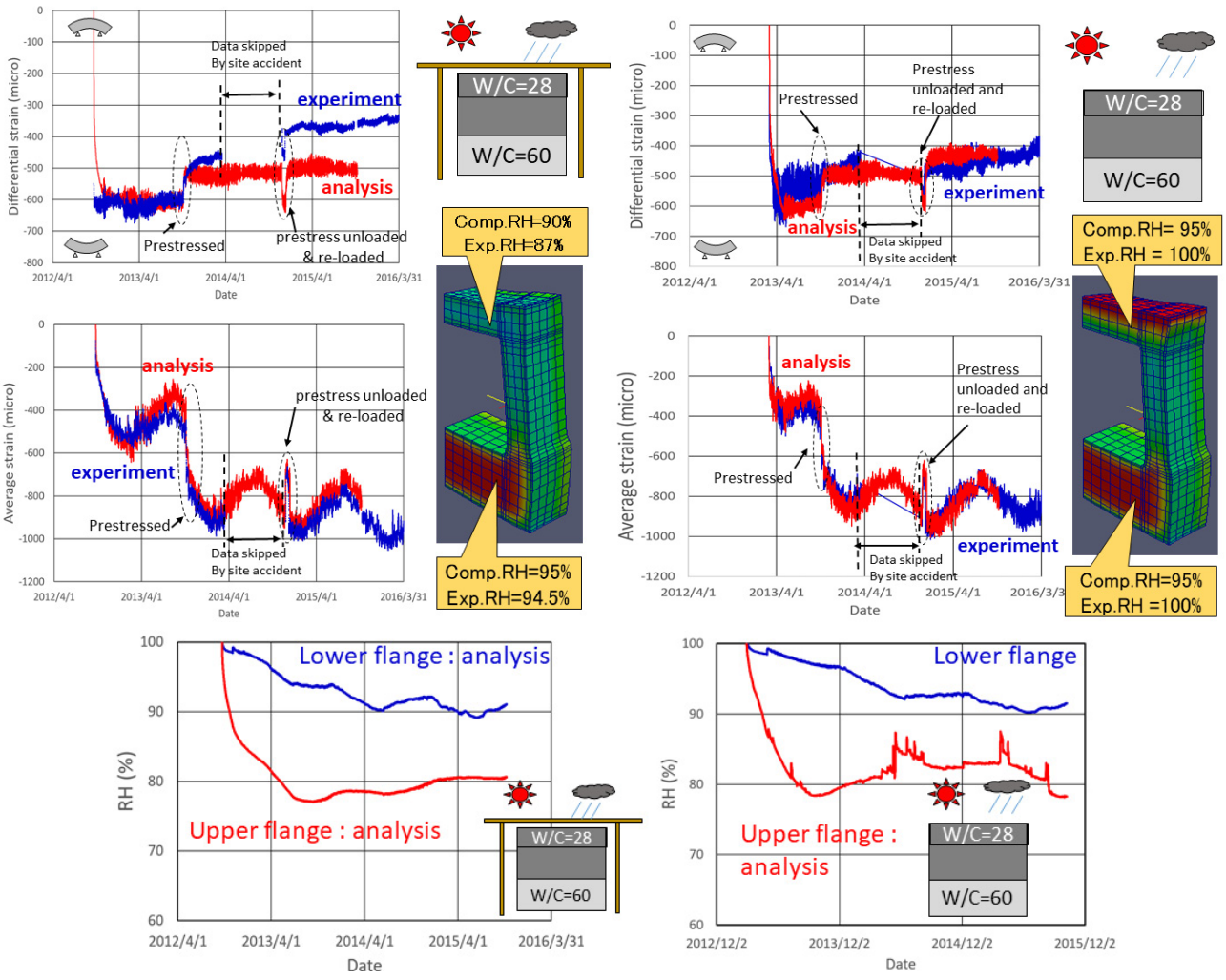

(a) Sectional deformation of Unit-2 with and without roof cover.

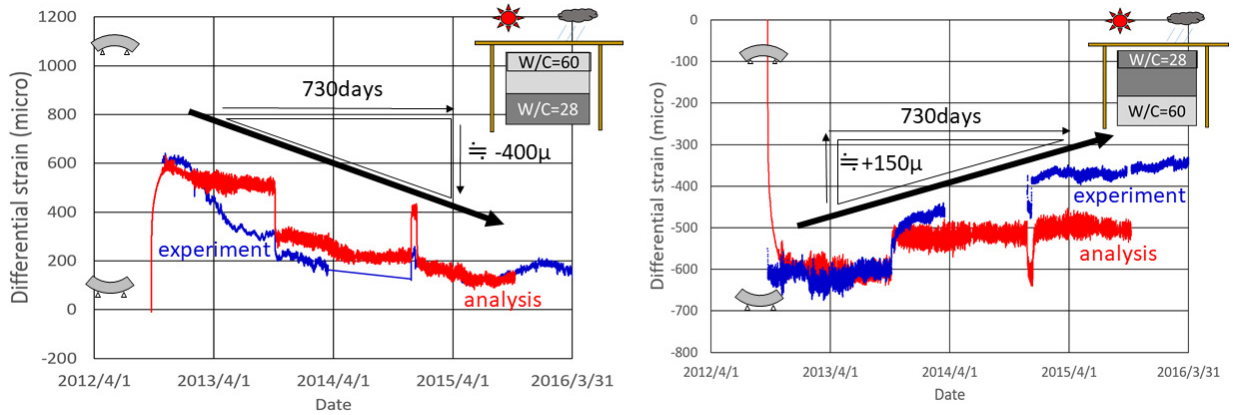

(b) Comparison of warping recovery between Unit-2 and Unit-1

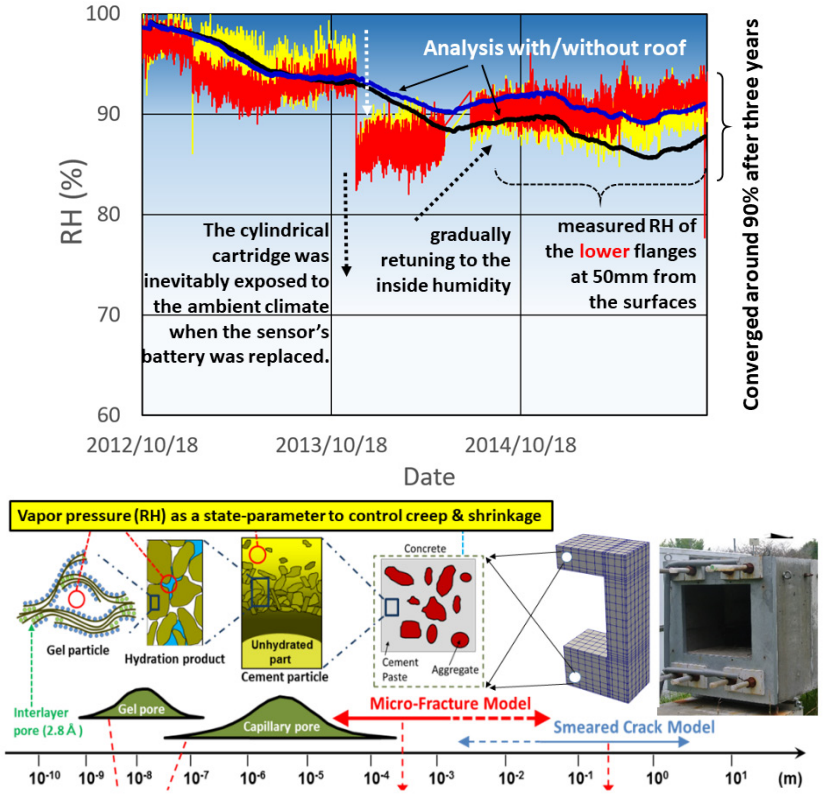

(c) Converged relative humidity inside concrete flanges and comparison with site measurement

Fig. 14 Transient differential and average axial strains with the internal humidity inside mockup Unit-2.

averaged natural environments in Japan.

(3) The thermo-hygral multi-scale modeling was applied for lifetime simulation of the targeted mockup specimens and its applicability was confirmed. Here, the rapid suction and bulk motion of condensed water caused by yearly precipitation was treated as non-quasi equilibrium process by tentatively magnifying the vapor transmission characteristics.

Acknowledgement

The authors express their gratitude to Dr. T. Mishima and Mr. J. Arita of Maeda Corporation for his support to build the site measurement unit and to produce PC segments. Their appreciation is extended to Mr. Y. Fujieda of Kakioka Test Site of The University of Tokyo, for his long lasting assistance, valuable advices and suggestions. The authors sincerely thank Mr. T. Miyasato, Mr. Y. Tominaga, Mr. H. Kono and Mr. T. Kanuma for their facility management and continuous measurement. The special thanks are addressed to Prof. M. Iwanami of Tokyo Institute of Technology for his long-term supports and advises. This research is financially supported by MEX/JSPS KAKENHI 23226011.

References

Al-Saleh, S. A. and Al-Zaidb, R. Z., (2006). "Effects of drying conditions, admixtures and specimen size on shrinkage strains." *Cement and Concrete Research*, 36(10), 1985-1991.

Andrade, C., Sarria, J. and Alonso, C., (1999). "Relative humidity in the interior of concrete exposed to natural and artificial weathering." *Cement and Concrete Research*, 29(8), 1249-1259.

Asamoto, S., Ohtsuka, A., Kuwahara, Y. and Miura, C., (2011). "Study on effects of solar radiation and rain on shrinkage, shrinkage cracking and creep of concrete." *Cement and Concrete Research*, 41(6), 590-601.

Asamoto, S., Ishida, T. and Maekawa, K., (2008). "Investigations into volumetric stability of aggregates and shrinkage of concrete as a composite." *Journal of Advanced Concrete Technology*, 6(1), 77-90.

Asamoto, S., Ishida, T. and Maekawa, K., (2006). "Time-dependent constitutive model of solidifying concrete based on thermodynamic state of moisture in fine pores." *Journal of Advanced Concrete Technology*, 4(2) 301-323.

Barr, P. J., Stanton, J. F. and Eberhard, M. O., (2005). "Effects of temperature variations on precast, prestressed concrete bridge girders." *Journal of Bridge Engineering*, ASCE, 10(2), 186-194.

Bažant, Z. P., Wendner, R., Hubler, M. H. and Yu, Q., (2012). "Pervasive lifetime inadequacy of long-span box girder bridges and lessons for multi-decade creep prediction." *The 3rd International Symposium on Life-Cycle Civil Engineering*, IALCCE.

Bažant, Z. P., Yu, Q., Li, G.-H., Klein, G. and Kristek, V., (2010). "Excessive deflections of record-span prestressed box girder." *Concrete International*, 32(6).

Bažant, Z. P., (2001). "Prediction of concrete creep and shrinkage: past, present and future." *Nuclear Engineering and Design*, 203, 27-38.

Burdet, O., (2010). "Experience in the long-term monitoring of bridges." *3rd fib International Congress*, 663, Washington D.C., USA, 108-113.

Burdet, O. and Baudoux, M., (1999). "Long-term deflection monitoring of pre-stressed concrete bridges retrofitted by external post-tensioning - examples from Switzerland." IABSE Rio, Rio de Janeiro, Brazil.

Chijiwa, N. and Maekawa, K., (2015). "Thermo-hygral case-study on full scale RC building under corrosive environment and seismic actions." *Journal of Advanced Concrete Technology*, 13, 465-478.

Chijiwa, N., Zhu, X., Ohno, H., Tanabe, S., Nakarai, K. and Maekawa, K., (2015). "Delayed shear crack formation of shallow RC box culverts in service." *CONCREEP 10, Mechanics and Physics of Creep, Shrinkage and Durability of Concrete and Concrete Structures*, 1579-1586.

Chiu, H. S., Chern, J. C. and Chang, K. C., (1996). "Long-term deflection control in cantilever prestressed concrete bridges. I: control method." *Journal of Engineering Mechanics*, 122(6).

Grasley, Z. C., Lange, D. A. and D'Ambrosia, M. D., (2006). "Internal relative humidity and drying stress gradients in concrete." *Materials and Structures*, 39, 901.

Han, X., An, X. and Maekawa, K., (2017). "Hygro-gradient model for permeability of unsaturated cementitious composites." *Journal of Advanced Concrete Technology*, 15(8), 407-425.

Hata, Y., Oonishi, N. and Watanabe, Y., (1993). "Creep behavior of pre-stressed concrete bridge over ten years." *Proc. of FIP symposium*, 305-310.

Ishida, T., Maekawa, K. and Kishi, T., (2007). "Enhanced modeling of moisture equilibrium and transport in cementitious materials under arbitrary temperature and relative humidity history." *Cement and Concrete Research*, 37(2), 565-578.

Ishida, T., Chaube, R. P., Kishi. T. and Maekawa, K., (1998). "Micro-physical approach to coupled authogenous and drying shrinkage of concrete." *Autogenous Shrinkage of Concrete* In: E. Tazawa Eds. Japan Concrete Institute, E & FN Spon.

Jauregui, D. V., White, K. R., Woodward, C. B. and Leitch, K. R., (2003). "Noncontact photogrammetric measurement of vertical bridge deflection." *Journal of Bridge Engineering*, ASCE, 8(4), 212-222.

Kim, J. K. and Lee, C. S., (1999). "Moisture diffusion of concrete considering self-desiccation at early ages." *Cement and Concrete Research*, 29(12), 1921-1927.

Kim, J. K. and Lee, C. S., (1998). "Prediction of differential drying shrinkage in concrete." *Cement and Concrete Research*, 28(7), 985-994.

Kristek, V., Baznt, Z. P., Zich, M. and Kohoutkova, A., (2006). "Box girder bridge deflections; Why is the initial trend deceptive?" *ACI Concrete International*, 28(1), 55-63.

Kunieda, M., Chijiwa, N., Ohara, K. and Maekawa, K., (2012). "Feasibility study of autonomous deformation control of PC viaducts." *From Materials to Structures - Advancement through Innovation* -." Samali, Attard & Song (Eds), Taylor & Francis Group, London (ISBN 978-0-415-63318-5), 313-318.

Kurihara, R., Chijiwa, N. and Maekawa, K., (2017). "Thermo-hygral analysis on long-term natural frequency of RC buildings with different dimensions." *Journal of Advanced Concrete Technology*, 15(8), 381-396.

Lura, P., Breugel, K. V. and Maruyama, I., (2002). "Autogenous and drying shrinkage of high-strength lightweight aggregate concrete at early ages–The effect of specimen size." PRO 23: *Early Age Cracking*, 335-342.

Mabrouk, R., Ishida, T. and Maekawa, K., (2004). "A unified solidification model of hardening concrete composite for predicting the young age behavior of concrete." *Cement and Concrete Composite*, 26, 453-461.

Mabrouk, R. T., Ishida, T. and Maekawa, K., (1998). "Solidification model of hardening concrete composite for predicting autogenous and drying shrinkage." *Autogenous Shrinkage of Concrete* In: E. Tazawa Eds. Japan Concrete Institute, E & FN Spon.

Maekawa, K., Zhu, X., Chijiwa, N. and Tanabe, S., (2016). "Mechanism of long-term excessive deformation and delayed shear failure of underground RC box culverts." *Journal of Advanced Concrete Technology,* 14(5), 183-204.

Maekawa, K., Ishida, T., Chijiwa, N. and Fujiyama, C., (2015). "Multiscale coupled-hygromechanistic approach to the life-cycle performance assessment of structural concrete." *Journal of Materials in Civil Engineering*, ASCE, 27(2), A4014003.

Maekawa, K., Suryanto, B., Fujiyama, C. and Chijiwa, N., (2012). "Microstructure based life-cycle assessment and durability design of concrete bridges (invited plenary)." *The 2nd International Conference on Microstructural-related Durability of Cementitious Composites.*

Maekawa, K., Chijiwa, N. and Ishida, T., (2011). "Long-term deformational simulation of PC bridges based on the thermo-hygro model of micro-pores in cementitious composites." *Cement and Concrete Research*, 41(12), 1310-1319.

Maekawa, K., Ishida, T. and Kishi, T., (2008). "*Multi-Scale modeling of structural concrete*." London, Taylor and Francis.

Maekawa, K., Pimanmas, A. and Okamura, H., (2003). "*Nonlinear mechanics of reinforced concrete*." London, Spon Press.

Maekawa, K., Ishida, T. and Kishi, T., (2003). "Multi-scale modeling of concrete performance -Integrated material and structural mechanics (invited)." *Journal of Advanced Concrete Technology*,

1(2), 91-126.

Maaddawy, T. E., Soudki, K. and Topper, T., (2005). "Long-term performance of corrosion-damaged reinforced concrete beams." *ACI Structural Journal*, 102(5), 649-656.

Mihashi, H., Maekawa, K, Ishida, T., Asamoto, S. and Maruyama, I., (2009). "Multi-scale modeling to link observed behavior, characterization and analysis." *Creep, Shrinkage and Durability Mechanics of Concrete and Concrete Structures*, 1, CRC Press, 117-143.

Nagataki, S. and Yonekura, A., (1984) "The mechanisms of drying shrinkage and creep of concrete." *Concrete Library International*, JSCE, 3, 177-191. (in Japanese)

Nakamura, K., Fukuyoshi, T. and Moriya, M., (1982). "Construction of the Tsukiyono Bridge by the P&Z method." *Concrete Journal*, JCI, 20(1). 38-44. (in Japanese)

Navrátil, J. and Zich, M., (2010). "Long-term deflections of long-span bridges." *Challenges, Opportunities and Solutions in Structural Engineering and Construction* – Ghafoori, ed. Taylor & Francis Group, London.

Ohno, M., Chijiwa, N., Suryanto, B. and Maekawa, K., (2012). "An investigation into the long-term excessive deflection of PC viaducts by using 3D multi-scale integrated analysis." *Journal of Advanced Concrete Technology*, 10, 47-58.

Pickett, G., (1942). "The effect of change in moisture content on the creep of concrete under a sustained load." *Journal of American Concrete Institute*, 38, 333-355.

Rodrigues, C., Félix, C., Lage, A. and Figueiras, J., (2010). "Development of a long-term monitoring system based on FBG sensors applied to concrete bridges." *Engineering Structures*, 32(8), 1993-2002.

Sakata, K., (1983). "A study on moisture diffusion in drying and drying shrinkage of concrete." *Cement and Concrete Research*, 13(2), 216-224.

Shimomura, T., (2015). "Simulation of long-term stress and deflection of concrete structures based on precise considerations of environmental action." *10th International Conference on Mechanics and Physics of Creep, Shrinkage, and Durability of Concrete and Concrete Structures (CONCREEP 10)*

Tazawa, E. and Miyazawa, S., (1995). "Experimental study on mechanism of autogenous shrinkage of concrete." *Cement and Concrete Research*, 25(8), 1633-1638.

Watanabe, Y., Ohura, T., Nishio, H. and Tezuka, M., (2008). "Practical prediction of creep, shrinkage and durability of concrete in Japan." *Creep, Shrinkage and Durability Mechanics of Concrete and Concrete Structures. Proceedings of the CONCREEP 8 Conference*, Ise-Shima 30 September-2 October 2008, Florida: CRC Press, 529-536.

Weiss, W. J., Yang, W. and Shah, S. P., (2000). "Influence of specimen size/geometry on shrinkage cracking of rings." *Journal of Engineering Mechanics,* 126(1).

Yoneda, T., Ishida, T., Maekawa, K., Gebreyouhannes, E., Mishima, T., (2015). "A micro-cracking model coupled with micro fracture and water status in micro pore structures." *Journal of Japan Society of Civil Engineers*, Ser. E2 (Materials and Concrete Structures), 71(3), 263-282.

Yoneda, T., Ishida, T., Maekawa, K., Gebreyouhannes, E. and Mishima, T., (2013). "Simulation of early-age cracking due to drying shrinkage based on a multi-scale constitutive model." *Poromechanics V*: ASCE, 579-588.